Journal of Materials Chemistry

Cite this: J. Mater. Chem., 2012, 22, 3752

www.rsc.org/materials

PAPER

Soft lithographic patterning of spin crossover complexes. Part 2: stimuli-responsive diffraction grating properties†

Amal Akou,[a] Il'ya A. Gural'skiy,[ab] Lionel Salmon,[a] Carlos Bartual-Murgui,[c] Christophe Thibault,[c] Christophe Vieu,[c] Gábor Molnár*[a] and Azzedine Bousseksou*[a]

Received 4th November 2011, Accepted 22nd December 2011
DOI: 10.1039/c2jm15663f

Surface-relief diffraction gratings of various geometries were fabricated from the molecular spin crossover complex $[Fe^{II}(hptrz)_3](OTs)_2$ using the soft lithographic method described in Part 1 of this paper [Quintero *et al.*, *J. Mater. Chem.*, DOI: 10.1039/c2jm15662h]. The grating geometry and optical properties were obtained from atomic force microscopy and spectroscopic ellipsometry measurements. The grating diffraction efficiency (η) was determined as a function of the temperature at various wavelengths (400–700 nm) using a conoscopic microscopy setup. A significant effect of the molecular spin state change on η is demonstrated (*ca.* 3% modulation). Using scalar transmission theory the changes in the diffraction pattern were quantitatively traced back to the decrease of the real part of the refractive index ($\Delta n_{HL} = -0.01$) accompanying the $^1A \rightarrow {}^5T$ spin transition. These stimuli-responsive photonic devices exhibit useful properties for various applications. Here a proof of concept gas sensor application is demonstrated for the detection of alcohol vapor.

Introduction

Spin crossover (SCO) complexes of $3d^4$–$3d^7$ transition metal ions represent an important class of bistable materials for which switching between high-spin (HS) and low-spin (LS) electronic configurations can be obtained by diverse external stimuli such as temperature, pressure, light irradiation, magnetic fields or even the adsorption of gas/vapour molecules.[1,2] The switching of molecular spin-states is accompanied by a spectacular change of various physical properties. For this reason the possible applications of these materials, including information storage, display and switching devices, pigments and sensors, continue to draw much attention. Up to now, efforts have been focused primarily on magnetic susceptibility and color changes. On the other hand, the refractive index changes associated with the SCO provide also interesting prospects for a range of photonic applications. The relevance of this property has been less widely recognized,[3–7] probably due to the lack of suitable thin films and photonic structures exhibiting SCO. Recently, however, considerable progress has been made in the synthesis of SCO nano-materials as patterned or continuous thin films, nano-composites or nanoparticles.[2] In particular, in Part 1 of the present paper we have described a simple, but efficient method to pattern regular arrays of micrometric and nanometric objects of the spin crossover complex $[Fe(hptrz)_3](OTs)_2$ (**1**) (*hptrz* = 4-heptyl-1,2,4-triazole and OTs = tosylate) using a soft lithography approach.[8] Furthermore, in a recent communication we have also revealed—using surface plasmon resonance detection—the significant refractive index changes accompanying the SCO phenomenon in thin films of **1**.[7] Based on these advances, in the present paper we propose a proof of concept for the photonic application of SCO nano-materials. To this aim we have elaborated and investigated diffraction gratings of **1**, wherein the modulation of the spin state of the complex leads to a substantial change of the diffraction pattern. Since the spin transition in compound **1** takes place just above room temperature,[9] these results provide a genuine scope for practical applications.

Experimental

Fabrication of diffraction gratings of $[Fe(hptrz)_3](OTs)_2$

Regular surface patterns of **1** were elaborated using polydimethylsiloxane (PDMS) stamps by the same method as described in ref. 8. The only difference was the use of photolithography instead of electron-beam lithography for the generation of the silicon master with micrometric patterns.[10]

Physical measurements

Spectroscopic ellipsometry measurements were performed in air by means of a Horiba-JobinYvon UVISEL apparatus and the

[a]*LCC, CNRS & Université de Toulouse (UPS, INP), 205 route de Narbonne, 31077 Toulouse, France. E-mail: gabor.molnar@lcc-toulouse.fr; azzedine.bousseksou@lcc-toulouse.fr*
[b]*Department of Chemistry, National Taras Shevchenko University, 62 Vladimirska str., 01601 Kiev, Ukraine*
[c]*LAAS, CNRS & Université de Toulouse (UPS, INSA, IAES), 7 avenue du colonel Roche, 31077 Toulouse, France*

† Electronic supplementary information (ESI) available: Microscopy images of $[Fe(hptrz)_3](OTs)_2$ surface-relief gratings with various grating geometries. See DOI: 10.1039/c2jm15663f

results were analyzed with the Cauchy absorbance model as implemented in the software. The temperature of the sample was controlled with a thermoelectric device (Linkam PE120). Surface topographical characterization was performed at room temperature using a Digital Instruments Nanoscope IIIa atomic force microscope (AFM) operating in tapping mode. Conoscopic and orthoscopic images of the diffraction gratings were acquired in transmission mode using an optical microscope (Olympus BX51) equipped with a thermoelectrically cooled, megapixel format, 16 bit CCD camera (Andor Technology iKon-M DU934N-BV) and a ×5 magnification objective (numerical aperture, NA = 0.1). The gratings were illuminated by white light and the detected spectral range was reduced using band-pass filters (*ca.* 20 nm bandwidth). The sample temperature and atmosphere were controlled using a Linkam THMS600 liquid nitrogen cryo-stage. Prior to measurements the sample was dehydrated at 90 °C for 30 min under nitrogen flow in the cryostat and during the experiments the temperature was changed at a rate of 2 K min^{-1}. Gas absorption experiments were carried out as follows. An aliquot volume of liquid MeOH (2–19 μl) was placed into a 100 ml syringe. Following vaporization of the liquid phase at ambient temperature, the content of the syringe was introduced into a quartz cell containing the diffraction grating.

Results and discussion

Grating geometry

The surface-relief diffraction gratings of **1** were fabricated using a micro- or nano-patterned PDMS stamp as described in Part 1 of this paper.[8] The thickness (d) of the obtained patterns can be controlled by changing the concentration of the complex in the starting solution as well as by varying the PDMS stamp pattern depth, while the lateral size of the patterns is limited primarily by the lithography process used to fabricate the silicon master. The surface topography of the gratings has been characterized by AFM revealing continuous and homogeneous patterns over large areas (4 mm^2). Selected line and square gratings of **1** with different geometries are displayed in the ESI†. As an example, Fig. 1 shows the AFM topographic image of a 100 mm^{-1} line grating. The width of the lines ($f\Lambda$) and the grating period (Λ) determined from the AFM data are 4.5 (±0.1) μm and 10.0 (±0.2) μm, respectively.

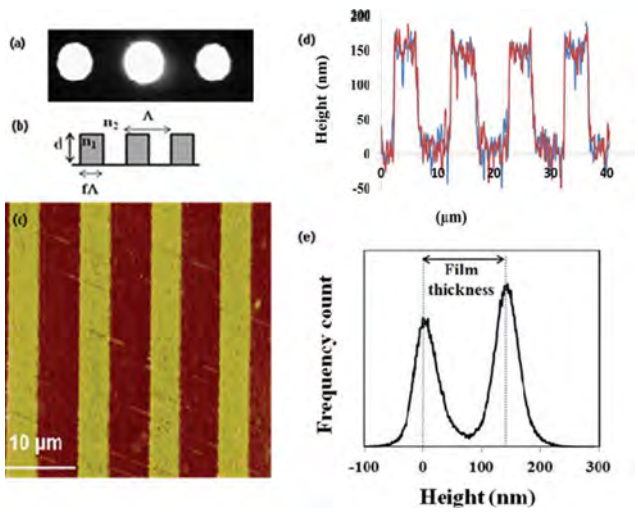

Fig. 1 (a) Diffraction pattern of a 100 lines per mm surface-relief grating of **1** ($m = 0, \pm1$, $\lambda = 700$ nm, NA = 0.1). (b) Schematic picture of the grating geometry. (c) AFM image, (d) height profile and (e) height distribution histogram of the grating.

While the overall geometry and the quality of the stamp are well reproduced, the fill factor ($f = 0.45$) was found to be somewhat lower when compared to the stamp ($f = 0.5$). This could be explained by the swelling of the PDMS stamp in contact with the chloroform solution. The thickness of the grating, determined from the AFM height distribution histogram, was found to be $d = 140$ nm (±15 nm) which is close to the nominal depth of the cavities in the stamp (*ca.* 150 nm). It may be useful to note that gratings with different periods but with the same thickness and fill factor are expected to display similar diffraction efficiencies (*vide infra*). The choice of a $\Lambda = 10$ μm grating for the present work is practical, because it allows us to use straightforward scalar diffraction theory, while keeping the diffracted orders angularly well resolved.

Diffraction efficiencies—experiment

The diffraction patterns of the gratings have been investigated in transmission geometry using an optical microscope.[11] According to the theory of Abbe,[12] the back focal plane of the microscope objective is also the Fourier plane of the image, hence the diffraction orders produced by a periodic grating structure can be straightforwardly observed by examining the objective aperture. To switch from the usual orthoscopic observation (*i.e.* direct view of the focused image of the specimen) to conoscopic observation (*i.e.* observation of the image formed at the back focal plane of the objective) we used a Bertrand lens, which serves basically as a telescope objective (Scheme 1). If the grating is illuminated by a narrow, partially coherent and monochromatic beam with wavelength λ—in our case using a bandpass filter and with the condenser aperture closed down—the number of diffraction orders (m) which can be visualized (provided they are not evanescent) is determined by the grating equation:

$$\mathrm{NA} \geq m\lambda/\Lambda \quad (1)$$

As an example, Fig. 1a depicts the diffraction image of a 100 mm^{-1} line grating. A useful figure of merit for diffraction gratings is the diffraction efficiency, which is defined for a given order as:

$$\eta_m = \frac{I_m}{I_{\mathrm{inc}}} \approx \frac{I_m}{\sum_{-\infty}^{+\infty} I_m} \quad (2)$$

where I_m and I_{inc} stand for the intensity of the diffracted light (m^{th} order) and the incident light beams, respectively. In our calculations we approximated I_{inc} by the sum of the intensity of the observed diffracted spots and that of the undiffracted, zero-order spot ($\sum_{-\infty}^{+\infty} I_m$). This leads to a minor error because we neglect the contributions from (very weak) undetected orders. This shortcoming is largely compensated, however, by the fact that this type of normalization provides not only immunity against various measurement errors (drifts, fluctuations, *etc.*),

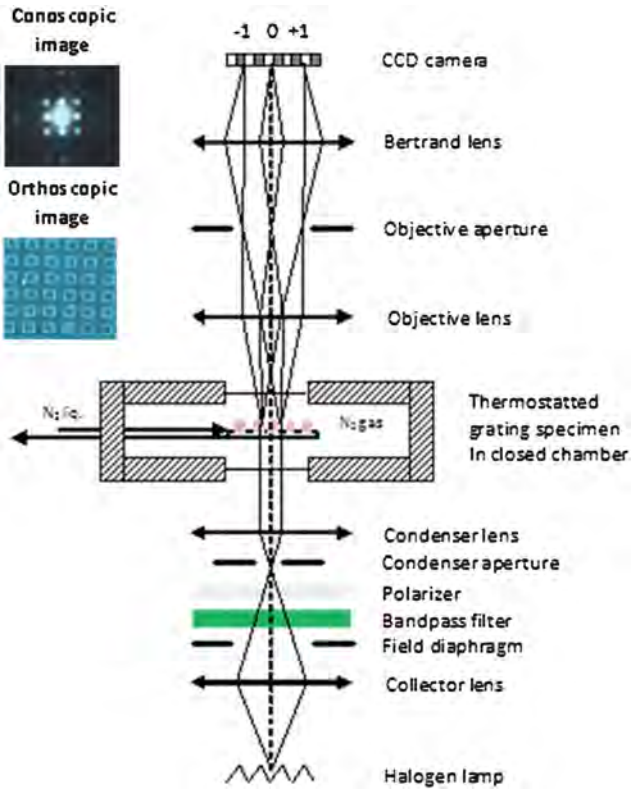

Scheme 1 Schematic representation of the optical microscopy setup used for variable-temperature diffraction measurements.

but reflection and scattering losses are also intrinsically corrected.

Changing the sample temperature is certainly the most straightforward way to induce spin state changes in molecular SCO complexes, therefore measurements of η_m were carried out using a variable-temperature cryo-stage. Our microscope based diffraction-imaging setup provides a significant advantage for variable-temperature work, because the thermal drift of the sample can be very accurately compensated in orthoscopic mode using the XYZ positioning stage of the microscope. The thermal evolution of the intensity of the zero- and first-order diffraction spots ($\lambda = 700$ nm) in the cooling and heating processes between 275 and 355 K is shown for a 100 mm^{-1} line grating of **1** in Fig. 2. One can observe a clear decrease of the first-order intensities while the zero-order intensity increases slightly. The corresponding evolution of the first-order diffraction efficiency is depicted in Fig. 3. Since the spin crossover behavior of our complex depends considerably on the degree of hydration a good reference is provided by the dehydrated complex (Fig. 3a). The same grating was also exposed to ambient air overnight to uptake humidity. The temperature-dependent behavior of this "hydrated grating" is shown for comparison in Fig. 3b. In both cases, the diffraction efficiency decreases with increasing the temperature, but an abrupt change of the diffraction efficiency is observed around $T_{1/2} = 312$ K (without measurable hysteresis) and around 330 K (with a hysteresis of 15 K) for the dehydrated and hydrated gratings, respectively. The thermal variation of the diffraction efficiency was perfectly reproducible over several thermal cycles proving that the decrease of η_1 is not related to sample degradation and/or dehydration. The overall shape of the $\eta_1(T)$ curves can be accounted for two phenomena: the spin transition and thermal expansion. In particular, the discontinuous change and the hysteresis loop are indicative of a first-order phase transition between the HS and LS forms of **1**. Within the hysteresis region the different values of η_m at a given temperature in the heating and cooling modes reflect obviously the spin state change, the difference being $\Delta\eta_1 \approx 0.15$ when going from the HS to the LS state. By subtracting the linear slopes before and after the transition we can extract a curve, which displays solely the spin state change induced effects (right panels in Fig. 3). The

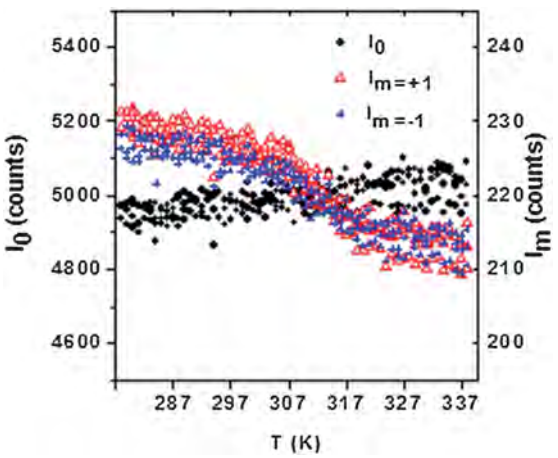

Fig. 2 Temperature dependence of the zero and first order diffraction intensities for a dehydrated grating of **1** ($\Lambda = 10$ μm, $d = 140$ nm, $\lambda = 700$ nm, $dT/dt = 2$ K min^{-1}) through two thermal cycles.

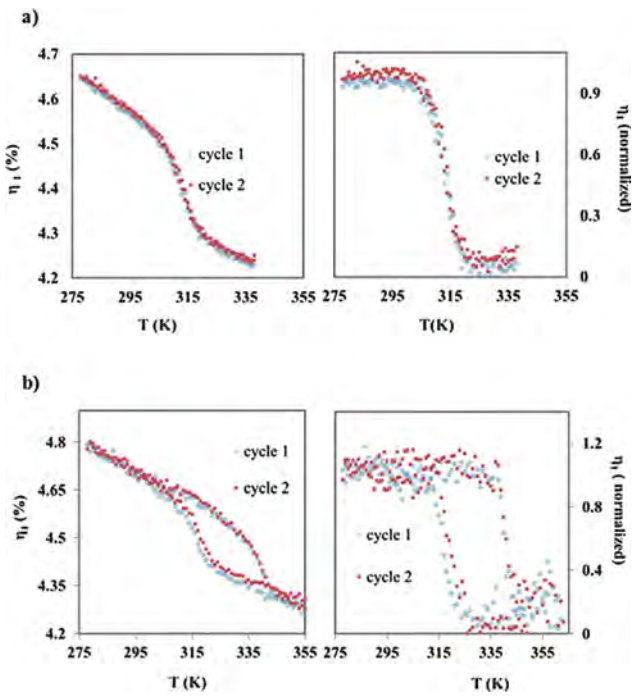

Fig. 3 Temperature dependence of the diffraction efficiency for a dehydrated (a) and hydrated (b) grating of **1** ($\Lambda = 100$ mm^{-1}, $d = 140$ nm, $\lambda = 700$ nm, $dT/dt = 2$ K min^{-1}) through two thermal cycles. Left panels: uncorrected data and right panels: data corrected for the thermal dilatation.

overall agreement between these spin transition curves and our previous luminescence measurements[8] on 80 nm thick dehydrated films of **1** is very good.

Diffraction efficiencies—theory

Grating behavior arises from the spatially periodic fluctuations of the complex refractive index ($n^* = n + ik$). In our case, the absorption effects for the 140 nm thick gratings are negligible in the whole visible and near-infrared wavelength range both in the HS and LS states. Indeed, the absorption spectra of **1** shown in Fig. 4 reveal only the presence of weak, spin-forbidden d → d transitions between 400 and 900 nm.

Our gratings should therefore exhibit an almost pure phase grating behavior. In order to check this hypothesis we have determined the real part of the refractive index n in a wide wavelength range using spectroscopic ellipsometry. As can be seen in Fig. 5a, n shows no singularity in the visible wavelength range. Only the classical dispersion is observed and this was found valid for the whole investigated temperature range. The temperature dependence of n at a few selected wavelengths is plotted in Fig. 5b (heating mode). The resemblance between the curves $\eta_m(T)$ and $n(T)$ is striking at first glance. In order to make a more quantitative comparison between the ellipsometry and diffraction data, we have calculated the theoretical diffraction efficiency using the ellipsometric data as input for the calculations. The diffraction efficiencies of transmission gratings may be calculated with high accuracy using the transmittance diffraction theory provided that the spatial frequency of the grating is much higher than the wavelength of the diffracted light ($\Lambda \gg \lambda$) and the thickness of the grating is small ($d < \lambda$).[13] These conditions are clearly fulfilled in our case. In this approach, the transmittance of the grating structure—which is a periodic function—is expanded into Fourier series. Then, the Fourier coefficients can be identified as the amplitudes of the diffracted waves. In the case of rectangular surface-relief gratings, the following analytical expressions are obtained for the diffraction efficiency for the zero and non-zero orders, respectively:[14]

$$\eta_{m=0} = 1 - 4f(1-f)\sin^2\left(\frac{\pi\Delta nd}{\lambda}\right) \quad (3)$$

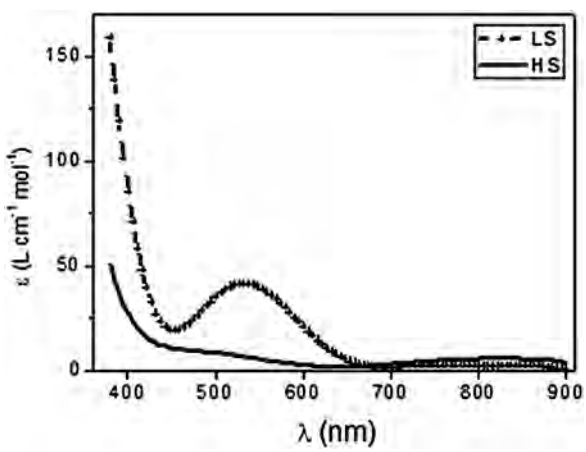

Fig. 4 Wavelength dependence of the molar absorption coefficient of **1** in the HS (320 K) and LS (293 K) states measured in chloroform solution.

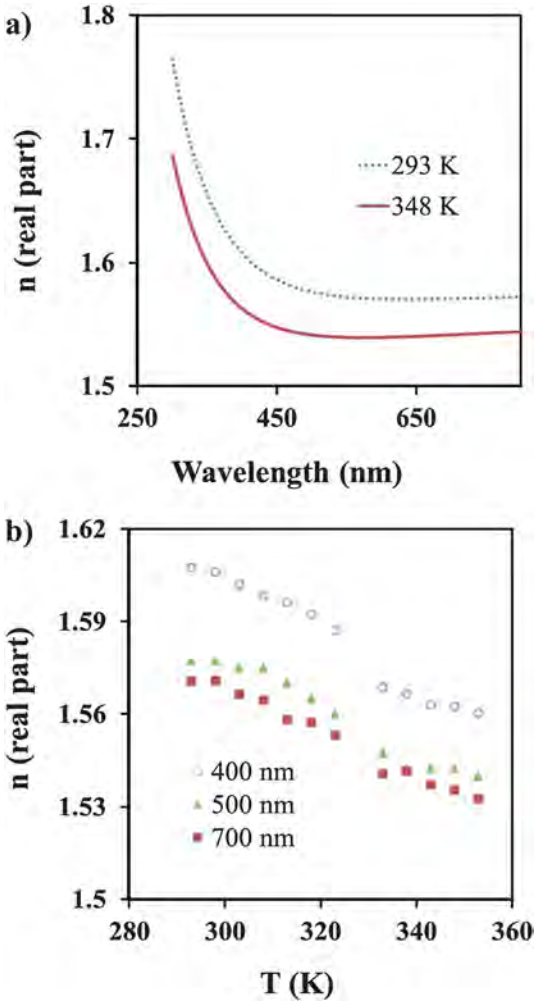

Fig. 5 Spectroscopic ellipsometry results: (a) refractive index spectra of a continuous thin film of **1** ($d = 80$ nm) in its hydrated form at 348 K (HS state) and at 293 K (LS state) and (b) temperature dependence of the real part of the refractive index in the heating mode at different wavelengths.

$$\eta_{m\neq 0} = \left[\frac{\sin(m\pi f)\sin\left(\frac{\pi\Delta nd}{\lambda}\right)}{m\pi/2}\right]^2 \quad (4)$$

In order to get more physical insights, one can simplify the last equation by approximating $\sin(\pi\Delta nd/\lambda) \approx \pi\Delta nd/\lambda$, which is legitimate in the thin film limit ($d \to 0$). Then, for $f = 0.5$ one obtains a simple expression (even orders have zero intensity):

$$\eta_{m=\text{odd}}\left[\frac{2\Delta nd}{m\lambda}\right]^2 \quad (5)$$

This means that the diffraction efficiency rises quadratically with increasing grating thickness and increasing refractive index modulation. One may also note that eqn (3) and (4) reveal opposite trends for the zero and non-zero orders in agreement with the data reported in Fig. 2.

Using eqn (4) with the grating geometrical parameters d and f determined by AFM as well as with the values of $n(T,\lambda)$ obtained

Table 1 First order diffraction efficiency at different wavelengths measured (Exp) and calculated (Theo) in the LS (293 K) and HS (338 K) states for a grating of **1**

	η_1 (%) 293 K	η_1 (%) 338 K
λ/nm	Theo/Exp	Theo/Exp
700	4.86/4.70	4.51/4.35
650	5.52/5.50	4.98/4.87
540	7.88/7.40	7.05/7.04
500	9.19/8.89	8.19/7.78
390	15.92/15.69	13.92/13.80

from ellipsometry, we have calculated the theoretically expected diffraction efficiencies for selected temperatures and wavelengths. Table 1 shows the calculated first order diffraction efficiencies (neglecting absorption and scattering losses) together with the experimentally obtained values of $\eta_1(T,\lambda)$. The overall agreement between theory and experiment is very good. In particular, one can observe that with increasing wavelength as well as with increasing temperature the diffraction efficiency decreases both in the experiment and in the theory. These results confirm thus our interpretation of the grating behavior in terms of refractive index changes. These diffraction data are also consistent with our surface plasmon resonance experiments on thin continuous layers of **1**,[7] providing thus the first reliable determination of the refractive index change upon SCO (Δn_{HL}) in a broad spectral range. (The data for the real part of n^* reported in ref. 4 are strongly hampered by light scattering on the powder sample.)

As explained in ref. 7, the primary origin of this refractive index modulation must be the volume expansion and associated density change, $\Delta\rho$, upon heating: $\Delta n(T)/n = \Delta\rho(T)/\rho$. Far from the transition temperature there is a nearly linear volume change associated with ordinary thermal dilatation.[15] The thermal expansion coefficients in the HS and LS phases are not the same, which explains the different slopes observed below and above the transition temperature (see Fig. 3). The spin transition involves also a considerable volume change due to the different population of anti-bonding e_g and non-bonding t_{2g} orbitals of the Fe^{II} ion (HS: $t_{2g}^4e_g^2$, LS: $t_{2g}^6e_g^0$). The volume of the octahedron defined by the six ligating nitrogen atoms around the iron(II) ion is typically 25–30% higher in the HS state (~10 Å^3 *vs.* ~13 Å^3) leading to a unit cell expansion $\Delta V/V$ between 1 and 10%, depending on the nature of the compound.[1] Unfortunately, the unit cell parameters of our compound could not be determined, but the observed refractive index change upon the spin transition $\Delta n_{HL}/n \approx 0.5$ to 1% gives some confidence that our description of these changes in terms of density modulation is a reasonable one. It is important to notice that the volume expansion leads inevitably to a variation of the sample thickness as well. Eqn (5) tells us that the increase of the grating thickness will compensate the decrease of the refractive index to some extent. Actually, the refractive index values determined from ellipsometry or from the diffraction measurements have not been corrected for this thickness change and should therefore considered as "effective values".

Application example

Diffractive optical components are widespread in spectroscopy, imaging, sensors, lasers and other optical systems. They are used as beam splitters, spectral filters, antireflection coatings, polarization devices, optical interconnects, *etc.*[14] Diffraction gratings based on spin crossover complexes can provide a significant added value for a multitude of applications. For example, the possibility to tune the diffraction efficiency can be used in beam dividers, while the refractive index tuning can be the basis for the construction of sub-wavelength devices with adjustable spectral or polarization properties. The fact that the molecular spin states can be inter-converted by light irradiation provides an interesting scope for photo-induced dynamic gratings.[3] Moreover, the existence of a thermal hysteresis loop in certain compounds gives rise to a non-volatile memory effect (Fig. 3b). On the other hand, optical diffraction can be also advantageously used for chemical sensing. The signal transduction principle is based on refractive index and/or grating geometry modulation upon the adsorption of the analyte molecules by the grating.[16,17] In this context, spin crossover materials may offer several advantages, including

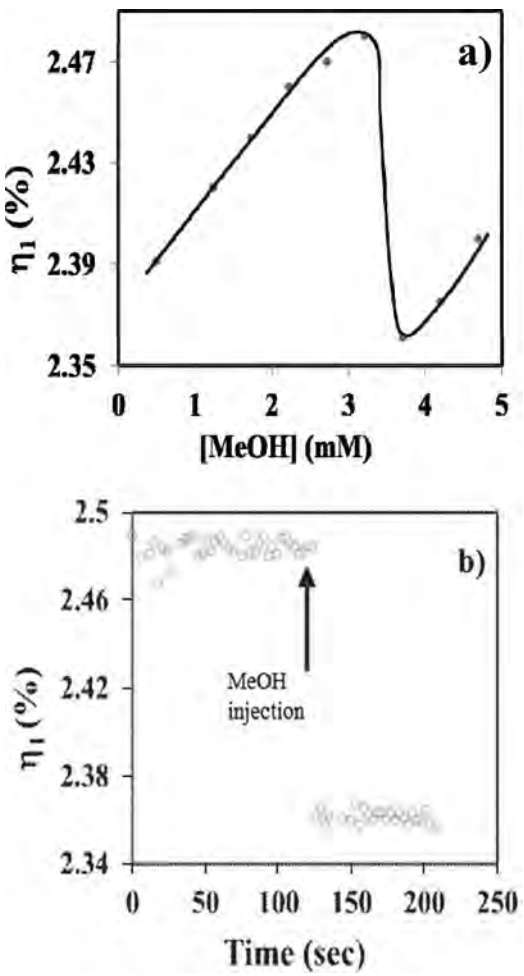

Fig. 6 (a) Diffraction efficiency of a grating of **1** upon exposure to increasing concentrations of methanol ($T = 298$ K, $\lambda = 700$ nm). The line is inserted to guide the eye. (b) Time-resolved variation of the diffraction efficiency when increasing the methanol concentration from 3.2 to 3.7 mM. The MeOH injection occurred at 110 s.

signal amplification and increased selectivity.[18] For example, in the case of **1** adsorption of water molecules stabilizes the LS form of the complex as it can be depicted from the comparison of Fig. 3a and b.

On the other hand, methanol adsorption stabilizes the HS form of the complex; the color of powder **1** turns from pink to colorless upon MeOH exposure. We have carried out thus a series of experiments in which methanol vapor was injected in various concentrations onto a grating of **1** at room temperature (Fig. 6). The modulation of the diffraction efficiency as a function of the methanol vapor concentration is reported in Fig. 6a. Initially, one can observe a quasi-linear increase of the diffraction efficiency from 2.39% to 2.48% with increasing MeOH concentration. This is the classical grating response: the uptake of molecules by the grating leads to an increase of its refractive index and thus higher diffraction efficiency.[16] However, between *ca.* 3.2 and 3.7 mM a sudden drop of η_1 is observed from 2.48% to 2.36%. Around this critical MeOH concentration the HS phase becomes thus thermodynamically stable and an abrupt LS → HS spin transition occurs leading to reduced diffraction intensity. This is depicted in more detail in Fig. 6b. Finally, further MeOH adsorption by the HS phase leads again to increasing values of η_1. This grating response is reversible: after desorbing the methanol molecules the grating recovers its initial spin state. Clearly, this experiment does not provide a ready-to-use sensor concept, but it does demonstrate the potential use of SCO compounds to obtain specific sensor responses, such as the detection of a threshold concentration of an analyte. Note, however, that this threshold behavior is related most likely to the very cooperative nature of the spin transition in **1** and a less cooperative system is expected to give a more gradual response.

Conclusion

In summary, diffraction gratings have been fabricated from a spin crossover complex by means of soft lithography and a significant effect of the molecular spin state change on the grating diffraction efficiency has been demonstrated. Using transmittance theory, the variation of the diffraction efficiency was traced back quantitatively to the large refractive index change ($\Delta n_{LH} \approx 10^{-2}$) accompanying the spin crossover. In the case of our test compound [Fe(*hptrz*)$_3$](OTs)$_2$ the refractive index changes in the visible wavelength range occur primarily due to the variation of the density of the material upon the spin transition. This means that every SCO material is expected to display this type of tunable grating behavior, since the SCO is always accompanied by a significant volume change. However, the magnitude of the refractive index modulation (both the real and imaginary parts) can be even higher close to electronic resonances (in particular in the vicinity of intense charge transfer transitions), while the overall grating efficiency can be also increased by using blazed gratings.[14]

These SCO gratings can respond reversibly to various external stimuli with fast response times. The response can be either transient (gating) or non-volatile (switching)—depending on the compound and on the experimental conditions. We believe that these assets provide a clear technological interest for tunable SCO gratings in a variety of applications including optics, photonics and chemical sensors.

The other way around, optical diffraction measurements (and other detection methods, which rely upon changes in the refractive index) can be advantageously used to investigate the spin crossover phenomenon in nano-scale materials, which is a burgeoning, though very challenging, topic at the moment.[2]

Acknowledgements

This work was financially supported by the project CHEMOSWITCH (ANR-10-BLAN-1018-01) and PRES—Université de Toulouse.

Notes and references

1 P. Gütlich and H. Goodwin, *Top. Curr. Chem.*, 2004, **233**, 1.
2 A. Bousseksou, G. Molnar, L. Salmon and W. Nicolazzi, *Chem. Soc. Rev.*, 2011, **40**, 3313.
3 A. Hauser, *Chem. Phys. Lett.*, 1993, **202**, 173.
4 E. D. Loutete-Dangui, F. Varret, E. Codjovi, P. R. Dahoo, H. Tokoro, S. Ohkoshi, C. Eypert, J.-F. Létard, J. M. Coanga and K. Boukheddaden, *Phys. Rev. B: Condens. Matter Mater. Phys.*, 2007, **75**, 184425.
5 P. Mounaix, E. Freysz, J. Degert, N. Daro, J.-F. Létard, P. Kuzel, V. Vigneras and L. Oyenhart, *Appl. Phys. Lett.*, 2005, **87**, 244103.
6 P. Mounaix, N. Lascoux, J. Degert, E. Freysz, A. Kobayashi, N. Daro and J.-F. Létard, *Appl. Phys. Lett.*, 2006, **89**, 174105.
7 G. Félix, K. Abdul-Kader, T. Mahfoud, I. A. Gural'skiy, W. Nicolazzi, L. Salmon, G. Molnár and A. Bousseksou, *J. Am. Chem. Soc.*, 2011, **133**, 15342.
8 C. M. Quintero, I. A. Gural'skiy, G. Molnár, L. Salmon, C. Bergaud and A. Bousseksou, *J. Mater. Chem.*, DOI: 10.1039/c2jm15662h.
9 O. Roubeau, J. M. Alcazar Gomez, E. Balskus, J. J. A. Kolnaar, J. G. Haasnoot and J. Reedijk, *New J. Chem.*, 2001, **25**, 144.
10 C. Thibault, G. Molnar, L. Salmon, A. Bousseksou and C. Vieu, *Langmuir*, 2010, **26**, 1557.
11 L. V. Kondrachova, R. A. May, C. W. Cone, D. A. Vanden Bout and K. J. Stevenson, *Langmuir*, 2009, **25**, 2508.
12 H. Köhler, *Optica Acta: International Journal of Optics*, 1981, **28**, 1691.
13 T. K. Gaylord, *Proc. IEEE*, 1985, **37**, 894.
14 R. Magnusson and D. Shin, Diffractive Optical Components, in *Encyclopedia of Physical Science and Technology*, Academic Press, New York, USA, 2002, vol. 4, pp. 421–440.
15 C. Kittel, *Introduction to Solid State Physics*, John Wiley & Sons Inc., New York, USA, 2005.
16 R. C. Bailey and J. T. Hupp, *J. Am. Chem. Soc.*, 2002, **124**, 6767.
17 J. C. Cau, H. Lalo, C. Severac, J.-P. Peyrade, E. Trévisiol, V. Leberre, J.-M. Francois and C. Vieu, *Oncologie*, 2009, **11**, S148.
18 (*a*) M. Ohba, K. Yoneda, G. Agustí, M. Muñoz, A. B. Gaspar, J. A. Real, M. Yamasaki, H. Ando, Y. Nakao, S. Sakaki and S. Kitagawa, *Angew. Chem., Int. Ed.*, 2009, **48**, 4767; (*b*) C. Bartual-Murgui, A. Akou, L. Salmon, G. Molnár, C. Thibault, J. A. Real and A. Bousseksou, *Small*, 2011, **7**, 3385.